HHS Public Access

Author manuscript

Cancer Immunol Res. Author manuscript; available in PMC 2019 July 01.

Published in final edited form as:

Cancer Immunol Res. 2018 July ; 6(7): 870–880. doi:10.1158/2326-6066.CIR-17-0661.

Nanobody-antigen conjugates elicit HPV-specific antitumor immune responses

Andrew W Woodham[1,2,*], **Ross W Cheloha**[1,2], **Jingjing Ling**[1,3], **Mohammad Rashidian**[1,2], **Stephen C Kolifrath**[1], **Maia Mesyngier**[1], **Joao N Duarte**[4], **Justin M Bader**[3], **Joseph G Skeate**[5], **Diane M Da Silva**[5,6], **W Martin Kast**[5,6,7], and **Hidde L Ploegh**[1,*]

[1]Program in Cellular and Molecular Medicine, Boston Children's Hospital, Boston, MA

[2]Department of Pediatrics, Harvard Medical School, Boston, MA

[3]Department of Biology, Massachusetts Institute of Technology, Cambridge, MA

[4]Whitehead Institute for Biomedical Research, 9 Cambridge Center, Cambridge, MA

[5]Department of Molecular Microbiology & Immunology, University of Southern California, Los Angeles, CA

[6]Norris Comprehensive Cancer Center, University of Southern California, Los Angeles, CA

[7]Department of Obstetrics & Gynecology, University of Southern California, Los Angeles, CA

Abstract

High-risk human papillomavirus-associated cancers express viral oncoproteins (e.g., E6 and E7) that induce and maintain the malignant phenotype. The viral origin of these proteins makes them attractive targets for development of a therapeutic vaccine. Camelid-derived single-domain antibody fragments (nanobodies or VHHs) that recognize cell surface proteins on antigen-presenting cells (APCs) can serve as targeted delivery vehicles for antigens attached to them. Such VHHs were shown to induce $CD4^+$ and $CD8^+$ T-cell responses against model antigens conjugated to them via sortase, but antitumor responses had not yet been investigated. Here, we tested the ability of an anti-CD11b VHH (VHH_{CD11b}) to target APCs and serve as the basis for a therapeutic vaccine to induce $CD8^+$ T cell responses against HPV^+ tumors. Mice immunized with VHH_{CD11b} conjugated to an H-$2D^b$-restricted immunodominant E7 epitope ($E7_{49–57}$) had more E7-specific $CD8^+$ T cells compared to those immunized with $E7_{49–57}$ peptide alone. These $CD8^+$ T cells acted prophylactically and conferred protection against a subsequent challenge with HPV E7-expressing tumor cells. In a therapeutic setting, VHH_{CD11b}-$E7_{49–57}$ vaccination resulted in greater numbers of $CD8^+$ tumor-infiltrating lymphocytes compared to mice receiving $E7_{49–57}$ peptide alone in HPV^+ tumor-bearing mice, as measured by *in vivo* noninvasive VHH-based immune-positron emission tomography (immunoPET), which correlated with tumor regression and survival outcome.

[*]**Corresponding Authors**: Andrew W. Woodham, Program in Cellular and Molecular Medicine, Boston Children's Hospital, 1 Blackfan Circle, RB 06005A, Boston, MA 02115. Phone: 323-434-6011; andrew.woodham@childrens.harvard.edu, Hidde L. Ploegh, Program in Cellular and Molecular Medicine, Boston Children's Hospital, 1 Blackfan Circle, RB 06215, Boston, MA 02115. Phone: 617-919-1613; hidde.ploegh@childrens.harvard.edu.

Disclosure of Potential Conflicts of Interest

AWW, RWC, JJL, MR, SCK, MM, JND, JB, JGS, DMD, WMK, and HLP have no conflicts of interest to disclose.

Together, these results demonstrate that VHHs can serve as a therapeutic cancer vaccine platform for HPV-induced cancers.

Introduction

Prophylactic vaccination against human papillomavirus (HPV) using capsid protein-based virus-like particles (VLPs) elicits protective humoral immunity against subsequent viral exposure and can prevent HPV-induced malignancies (1). However, for economic, political, and cultural reasons, not all individuals at risk for HPV infection receive the vaccine (2, 3). Consequently, transmission of HPV and the attendant risk of malignancies remain major global concerns (4). HPV-induced malignancies are of viral origin, and as such are excellent immunological targets because viral antigens (Ags) are distinct from self-Ags. HPV type 16 (HPV16) is the most common oncogenic high-risk HPV strain (5), with its primary drivers of oncogenesis, the early genes E6 and E7, constitutively expressed in HPV-induced tumors (6), making them major targets of antitumor vaccination strategies (7). Although prophylactic vaccination with VLP-based vaccines is protective prior to HPV exposure, established HPV^+ tumors will require a vaccination approach that elicits early gene product-specific cytotoxic $CD8^+$ T cells to eradicate tumors. Targeted delivery of Ags to professional antigen-presenting cells (APCs) enhances immunity against the delivered Ags through the generation of Ag-specific $CD8^+$ T cells (8, 9). Here we explored single-domain antibody fragments (also known as nanobodies or VHHs) as a therapeutic vaccine platform to deliver and induce cellular immunity against such VHH-conjugated antigens in an HPV cancer model.

VHHs are derived from the variable region of heavy chain-only antibodies naturally present in the serum of camelids (10). They are the smallest antibody fragments that retain Ag specificity (11). Their small size confers a number of desirable properties, such as stability, solubility, ease of production and modification, short circulatory half-lives, and similarity to human immunoglobulin V region sequences (12, 13). We demonstrated that VHHs specific for immune cell surface proteins (i.e. MHC class II, CD36, and CD11b) can deliver conjugated Ags to APCs and elicit an immune response to them (14). An Ag conjugated to the anti-CD11b VHH (VHH_{CD11b} or DC13) raised the strongest $CD8^+$ T-cell response against a model peptide antigen derived from ovalbumin. CD11b is the α subunit of integrin $\alpha_M\beta_2$ (Mac-1), expressed on neutrophils, macrophages, myeloid dendritic cells (DCs), NK cells, and subsets of $CD8^+$ T cells and B cells (15). To conjugate an Ag to a specific site on the VHH, we installed a sortase A recognition motif near the C-terminus of the VHH, and used an enzymatic transacylation reaction to attach a triglycine-equipped peptide (G_3-peptide) containing the Ag of interest (16, 17). We thus conjugated an immunodominant HPV type 16 E7 Ag (HPV16 $E7_{49–57}$) to VHH_{CD11b} via a sortase A-catalyzed reaction (Fig. 1). This VHH-Ag conjugate was successful as a therapeutic vaccine in an HPV cancer model in mice.

Methods

All procedures were performed in accordance with institutional guidelines and approved by the Boston Children's Hospital Institutional Animal Care and Use Committee (IACUC protocol number 16-12-3328).

Antibodies and reagents

Rat anti-CD11b-PE (clone M1/70) was purchased from eBioscience (San Diego, CA). Anti-mouse H-2D^b, H-2K^b, and CD80 were purchased from BioLegend (San Diego, CA). Anti-mouse CD40 (clone 1C10) was purchased from Southern Biotech (Birmingham, AL). polyinosinic-polycytidylic acid (Poly(I:C)) and lipopolysaccharide (LPS) from *Escherichia coli* (*E.coli*) were purchased from Sigma Aldrich (St. Louis, MO).

Mice and cell culture

Specific pathogen-free female 6–8-week-old C57BL/6 mice were purchased from Jackson Laboratory (000664), and OT-I Rag-deficient (Rag$^{-/-}$) mice were purchased from Taconic Biosciences (2334-F). Tumor challenge studies were performed with the C3.43 HPV16-transformed murine cell line (18, 19). C3.43 cells were a gift from W Martin Kast, PhD and were maintained in Iscove's modified Dulbecco's medium (IMDM) supplemented with 10% heat-inactivated fetal bovine serum (IFS), 50 μM 2-mercaptoethanol, and 100 U/mL penicillin/streptomycin. Cells used for tumor challenges were cultured no longer than 2 weeks from original seed stocks before *in vivo* injection. The murine dendritic DC2.4 and B cell lymphoma A20 cell lines were obtained from the ATCC and maintained in RPMI 1640 supplemented with 10% IFS, 2 mM glutamine, MEM nonessential amino acids, 1 mM sodium pyruvate, 50 μM 2-mercaptoethanol, and 100 U/mL penicillin/streptomycin. DC2.4 cells were characterized as CD11b$^+$H-2D^{b+}H-2K^{b+}CD80$^+$ as assessed by cytofluorimetry (Fig. 2A and 3A). A20 cells did not express CD11b (Fig. 2A). DC2.4 and A20 cells routinely test positive for known DC and B cell markers (i.e. DEC-205 and CD19, respectively) as examined by FACS and are passaged no more than 5 times from cryopreserved stocks. All cell lines were found to be mouse pathogen free (and *Mycoplasma pulmonis* free) by IDEXX BioResearch pathogen testing.

Recombinant protein expression, peptide synthesis, and sortase reactions

Recombinant VHHs containing a sortase recognition motif and 5× His-tag for purification were expressed in WK6 *E.coli* overnight in Terrific Broth at 30°C after isopropyl β-D-thiogalactopyranoside induction (1 mM) at an OD_{600} of ~0.6 (sequences available in Supplemental Table 1). VHHs were harvested from the periplasm by osmotic shock and purified by adsorption to Ni-NTA beads (MCLab, San Francisco, CA), followed by size-exclusion chromatography on a Superdex 75 16/600 column (GE Healthcare, Piscataway NJ) in PBS or Tris-HCl (50 mM, pH 7.5). VHHs were then concentrated using centrifugal filters with a 10 kDa molecular weight cut-off (Millipore Sigma, UFC901024). G_3-TAMRA and G_3-RRAAYRAHYNIVTF were synthesized as described (20). G_3-AAYSIINFEKL was synthesized at the MIT Biopolymers & Proteomics Core Facility (Cambridge, MA). Heptamutant Ca^{2+}-independent sortase A from *Staphylococcus aureus* ($SrtA_{staph7M}$) was expressed with a 5× his-tag and purified following published procedures (20, 21). All sortase

reactions were performed in 50 mM Tris-HCl (pH 7.5) for 2 h at 20–25°C as described (20). The reagent concentrations were VHH (2 mg/mL or ~140 μM), 300 μM nucleophile (G_3-RRAAYRAHYNIVTF, etc.), and 10 μM $SrtA_{staph7M}$. Residual unconjugated VHH and $SrtA_{staph7M}$ were removed by adsorption to Ni-NTA beads (MCLab). Excess nucleophile was removed via centrifugal filters with a 10-kDa molecular weight cut-off (Millipore Sigma, UFC901024). Identity of the final products was confirmed by liquid chromatography-mass spectrometry (LC-MS) (Fig. 1).

In vitro experiments

For binding experiments, $CD11b^+$ DC2.4 cells or $CD11b^-$ A20 cells were incubated with different concentrations of TAMRA-labeled VHH_{CD11b} or VHH_{cont} (anti-GFP VHH) (22), or PE-labeled anti-CD11b mAb (M1/70-PE) for 30 min at 4°C, and washed. Mean fluorescence intensity (MFI) was assessed by cytofluorimetry. For competition binding experiments, DC2.4 cells were pre-incubated with unlabeled VHH_{CD11b} (10 μg/mL) for 30 min at 4°C, and then incubated with VHH_{CD11b}-TAMRA (1 μg/mL) or M1/70-PE for 30 min at 4°C. MFI was then assessed via cytofluorimetry after washing. For *in vitro* presentation assays, DC2.4 cells were treated with 100 nM $OVA_{257–264}$ (SIINFEKL), VHH_{cont}-$OVA_{257–264}$, or VHH_{CD11b}-$OVA_{257–264}$ for 1 h in complete medium at 37°C and then washed with PBS. Cells were then stimulated with LPS (1 μg/mL) in complete medium overnight at 37°C. The DC2.4 cells were then collected and seeded onto pre-coated 96-well enzyme-linked immunosorbent spot (ELISpot) plates (see ELISpot assay below), to which 10^5 splenocytes from a $RAG^{-/-}$ OT-I mouse were added and incubated for 24 h at 37°C (1 DC2.4 cell: 20 OT-I splenocyte). DC2.4 cells and OT-I splenocytes are both C57BL/6-derived. The number of $OVA_{257–264}$-specific interferon-γ (IFNγ)-secreting cells was then measured via IFNγ ELISpot assay (see below).

In vivo experiments

To evaluate the induction of HPV16 E7-specific T cells, wild-type C57BL/6 mice were injected intraperitoneally (IP) with 6 nmol VHH_{CD11b}, $E7_{49–57}$, or VHH_{CD11b}-$E7_{49–57}$ plus adjuvant (adjuvant: 50 μg Poly(I:C) + 50 μg agonistic anti-CD40), or adjuvant only. 14-days post-vaccination, spleens were harvested and anti-$E7_{49–57}$-specific $CD8^+$ T cells were enumerated by IFNγ ELISpot assay. In a similar experiment, mice were injected IP with 6 nmol VHH_{CD11b}-$E7_{49–57}$ or VHH_{cont} (anti-GFP VHH)-$E7_{49–57}$ plus adjuvant, or adjuvant only 14 days prior to IFNγ ELISpot assay. To evaluate the protective effects of the induced $CD8^+$ T cells, C57BL/6 mice were injected IP with adjuvant alone; adjuvant plus 6 nmol $E7_{49–57}$ or VHH_{CD11b}-$E7_{49–57}$ on days −21 and −7; or left untreated (n = 5 per group). Serum was collected on days −14 and −7 to assess anti-VHH responses (Supplemental Fig. 1). On day 0, mice were challenged with 3×10^5 C3.43 cells subcutaneously (SC). Tumor growth and overall survival were then monitored. For therapeutic studies, C57BL/6 mice were challenged with 3×10^5 C3.43 cells on day 0, resulting in palpable tumors by day 8, and then randomized. On day 8 and 15, mice received an IP injection with adjuvant alone; adjuvant plus 6 nmol $E7_{49–57}$ or VHH_{CD11b}-$E7_{49–57}$; or left untreated ($n = 8$ per group for the $E7_{49–57}$ and VHH_{CD11b}-$E7_{49–57}$ groups, and $n = 4$ for the untreated group). $CD8^+$ tumor-infiltrating lymphocytes (TILs) were evaluated via immunoPET on day 8. To evaluate immunological memory, mice with complete tumor regression from the $E7_{49–57}$ and

VHH_{CD11b}-$E7_{49–57}$ groups in the therapeutic study (n = 3 per group) were challenged with $3×10^5$ C3.43 cells contralaterally, and then tumor growth and overall survival were monitored.

ELISpot assay

IFNγ ELISpot assays were performed following published procedures (23). Briefly, 96-well ELISpot plates (BD ELISPOT Mouse IFNγ ELISPOT Set, BD Biosciences, San Jose, CA) were coated with an IFNγ capture antibody (BD Biosciences) in PBS overnight at 4°C and plates were blocked with complete medium for 2 h at room temperature (RT). For *in vitro* presentation experiments, DC2.4 cell/OT-I splenocyte cocultures were set-up in quadruplicate as described above. Negative control wells contained only DC2.4 cells. For *in vivo* experiments, splenocytes from vaccinated mice were added in triplicate to wells containing the H-$2D^b$-restricted $E7_{49–57}$ peptide (2 μg/mL) in complete medium or medium alone as a negative control. Positive control wells for all experiments contained 1× Cell Stimulation Cocktail (Invitrogen, Carlsbad, CA). Post splenocyte plating, ELISpot plates were incubated overnight at 37°C. After 24 hrs, plates were washed and incubated with a biotinylated IFNγ detection antibody (BD Biosciences) for 2 h, followed by streptavidin-horse radish peroxidase (BD Biosciences) for 1 h at RT. The plates were developed with 3-amino-9-ethyl-carbazole substrate (BD ELISPOT AEC Substrate Set) for 5 min and dried for at least 24 h. Spots were enumerated using the KS ELISpot analysis system (Carl Zeiss, Thornwood, NY), and the number of spots in negative control wells was subtracted from experimental wells to determine the number of spots above background.

ImmunoPET imaging and analysis

Radiolabeling of the anti-CD8 VHH with ^{89}Zr (VHH_{CD8}-^{89}Zr) was performed as described (Fig. 5D) (24). Specifically, VHH_{CD8} was conjugated to G_3-desferrioxamine (DFO)-azide via $SrtA_{staph7M}$. The azide group was used to install 20 kDa polyethylene glycol (PEG) moiety (as DBCO-PEG), which improves the quality of the PET signal seen with VHH_{CD8} *in vivo* (24). A volume of $^{89}Zr^{4+}$ stock solution (1.0 M oxalic acid adjusted to pH 6.8–7.5 using 2.0 M Na_2CO_3) corresponding to 1.0−1.5 mCi was added to 200 μL VHH_{CD8}-DFO solution (~2.0 mg of chelexed PEGylated-VHH_{CD8}-DFO in 0.5 M HEPES buffer, pH 7.5) in a 2 mL microcentrifuge tube, and the total volume was adjusted to 300 μL using 1.0 M oxalic acid. The reaction mixture was incubated for 60 min at RT with agitation, loaded onto a PD-10 size-exclusion column (GE Healthcare), and eluted with PBS. Radiolabeling of VHH_{CD11b} with ^{64}Cu (VHH_{CD11b}-^{64}Cu) was performed as described (25). In brief, VHH_{CD11b} was conjugated to G_3-NOTA via $SrtA_{staph7M}$. 400 μL VHH_{CD11b}-NOTA (20 μM in 200 mM NH_4OAc buffer; pH 6.5) was mixed with 75 μL $^{64}CuCl_2$ (~6 mCi in 200 mM NH_4OAc buffer; pH 6.5). The reaction mixture was incubated for 20 min at RT with agitation, loaded onto a PD-10 size-exclusion column (GE Healthcare), and eluted with PBS. PET-CT was performed following published procedures (25). Briefly, mice were anaesthetized using isoflurane, injected with 20–50 μCi radiolabeled VHH via the tail vain, and imaged by PET-CT 24 h later using a G8 PET-CT small animal scanner (PerkinElmer, Norwalk, CT). PET and CT acquisition was ~10 min and 1.5 min, respectively, per animal. Images were reconstructed using the manufacturer's software. Data were further analyzed and quantified using VivoQuant software (inviCRO Imaging Service and Software, Boston,

MA). PET signal values were converted to units of percentage of injected dose per gram by using as input the total radioactivity at the time of measurement with the preprocessing tool. CT scans overlaid with PET signals were used to generate 3D regions of interest (ROIs) to represent certain regions within each mouse (i.e. tumor or lymph node). Once all ROIs were generated, a table was exported containing statistical information, such as mean PET signal or variation for each ROI. TIL and lymph node (LN) intensity was defined as the PET signal observed from ^{89}Zr-labeled VHH_{CD8} at the ROI over background PET signal observed in muscle tissue ROI.

Statistical analyses

All statistical analyses were performed on GraphPad Prism version 7.0 (GraphPad Software Inc., San Diego, CA). One- and two-site hyperbolic binding curves were used to estimate the equilibrium dissociation constants (K_D values) with R-square values used as a metric to evaluate the quality of fit of the model to the data. Statistical significance for ELISpot assays, tumor growth curves, and $CD8^+$ TILs were assessed with two-tailed unpaired *t*-tests or ANOVA. Survival curves were assessed via the Kaplan-Meier method, with statistical significance determined by the log-rank (Mantel-Cox) test. Alternatively, two-tailed Fisher's exact tests were used to assess differences between outcomes among groups. Significance was defined as $P < 0.05$ for all experiments.

Results

Design of VHH-antigen constructs

Mouse models of E6/E7-positive tumors show that HPV Ag-specific T cells are few and comparatively poor at homing to and infiltrating tumor tissue, unless the tumor-bearing animal is vaccinated against agents containing or encoding the immunodominant E7-derived peptide, $E7_{49–57}$ (RAHYNIVTF) (26, 27). This peptide is recognized by $CD8^+$ T cells in H-$2D^b$-restricted fashion (18). Therefore, we synthesized the $E7_{49–57}$ peptide as a sortase A-ready nucleophile for conjugation to an anti-CD11b VHH (14). In between the G_3 motif at the N-terminus and the $E7_{49–57}$ epitope, two arginines (RR) were included to increase solubility; an AAY linker was added to enhance cross-presentation upon internalization by target APCs (28). The resultant sequence was GGGRRAAYRAHYNIVTF. Although standard genetic means are an obvious alternative to create the requisite fusions, the ability to multiplex enzymatic conjugations and extend this approach to multiple peptide or protein Ags affords flexibility, including the site-specific installation of post-translational modifications (20, 21) and radioisotopes for positron emission tomography (PET) (25). A genetic fusion would have to be purified from an appropriate source, where appendage of a C-terminal tag (e.g. a His tag) would be deployed for affinity enrichment. However, the presence of such C-terminal extensions would require further processing steps that would likely limit the generation of the relevant peptide epitope for MHC binding, as ER peptidases primarily trim N-terminal residues (29). Purification to homogeneity of the desired fusion in the absence of a tag may not always be possible. Because of the efficiency and specificity of sortase A-catalyzed reactions, we therefore applied the enzymatic approach, which yields the desired fusion in yield and purity. Accordingly, VHH_{CD11b} was expressed with a C-terminal sortase-recognition motif (LPETG) and 5× His-tag for

purification (Fig. 1 Ai). The E7 Ag nucleophile (G_3-RRAAYRAHYNIVTF) was site-specifically conjugated using sortase A and purified (Fig. 1 Aii–Aiii) as verified by liquid chromatography-mass spectrometry (LC-MS) (Fig. 1B–C). The purified VHH-Ag construct (VHH_{CD11b}-$E7_{49–57}$) was used in subsequent *in vivo* vaccination experiments.

VHH_{CD11b} specifically binds to $CD11b^+$ cells with high affinity

VHH_{CD11b} binds to the splenocytes of wild-type but not $CD11b^{-/-}$ mice (14). Here we show that VHH_{CD11b} binds to $CD11b^+$ DC2.4 cells, but not to $CD11b^-$ A20 cells (Fig. 2A). Competition assays with unlabeled VHH_{CD11b} showed that the fluorophore attached to VHH_{CD11b} did not affect its binding to DC2.4, and that VHH_{CD11b} binds an epitope different from that recognized by the well-established anti-mouse CD11b mAb M1/70 (Fig. 2B). Data from our binding studies fit substantially better to a two-site binding model compared to a one-site model (R^2 = 0.9895 and 0.6182, respectively), notwithstanding monovalency of VHH_{CD11b}. Paradoxically, M1/70 binding was well-modelled using a one-site binding model (R^2 = 0.9949) (Fig. 2C–D). As CD11b is a member of the integrin family capable of undergoing dramatic conformational changes, these results may indicate that VHH_{CD11b} recognizes two distinct conformations of CD11b, one with high affinity (K_{D1} of 0.204 ± 0.090 nM) and one with moderate affinity (K_{D2} = 110 ± 47 nM), whereas M1/70 binds the different conformers with equal affinity.

Cross-presentation of $OVA_{257–264}$ is increased when conjugated to VHH_{CD11b}

The efficacy of therapeutic vaccines against HPV-driven cancers lies in their ability to elicit strong $CD8^+$ T-cell responses against E6 and E7 proteins, which in the case of most peptide-based vaccines requires internalization, processing, and cross-presentation of the Ags on class I MHC (MHCI) (7). To explore the ability of VHH_{CD11b} to enhance Ag presentation, DCs were treated with an H-$2K^b$–restricted ovalbumin peptide ($OVA_{257–264}$) or an equivalent molar amount of peptide conjugated to VHH_{CD11b} (VHH_{CD11b}-$OVA_{257–264}$). $OVA_{257–264}$ was chosen for these experiments because no TCR transgenic mice are available that recognize HPV antigens to serve as a source of adequate numbers of E7-specific $CD8^+$ T cells. We measured the expression of relevant surface markers on the treated DCs after activation with LPS (Fig. 3A) and the corresponding $CD8^+$ T-cell responses following coculture of the differentially activated DCs with splenocytes from an OT-I $OVA_{257–26}$–specific T-cell receptor (TCR) transgenic mouse (30). Treatment with the VHH_{CD11b}-$OVA_{257–264}$ conjugate resulted in a greater than two-fold increase in the number of IFNγ-secreting effector $CD8^+$ T cells compared to peptide alone or peptide conjugated to a nontargeting control VHH (VHH_{cont}) (Fig. 3B–C). While exogenously added peptides can bind directly to cell surface MHCI, proteins when added at equimolar concentrations obviously still require processing and cross-presentation (31). These results show that VHH_{CD11b}-$OVA_{257–264}$ efficiently entered the cross-presentation pathway.

VHH_{CD11b}-$E7_{49–57}$ vaccination elicits stronger T cell responses than $E7_{49–57}$ alone

Vaccination with 30 nmol $E7_{49–57}$ peptide with the adjuvant poly(I:C) and an agonistic mAb to CD40 results in robust HPV-specific T-cell responses (32). Therefore, to assess the ability of VHH_{CD11b}-$E7_{49–57}$ to enhance HPV-specific T-cell responses *in vivo*, the dose of $E7_{49–57}$ peptide and VHH_{CD11b}-$E7_{49–57}$ was reduced to just 6 nmol, corresponding to ~100 μg of

VHH_{CD11b}-$E7_{49–57}$ injected per mouse. Mice were injected IP with VHH_{CD11b}, $E7_{49–57}$, or VHH_{CD11b}-$E7_{49–57}$ plus adjuvant (poly(I:C) and anti-CD40), or adjuvant only. Two weeks after vaccination, spleens were harvested and anti-$E7_{49–57}$ specific $CD8^+$ T cells were enumerated via IFNγ ELISpot assay. A single vaccination with VHH_{CD11b}-$E7_{49–57}$ resulted in a two-fold increase in the number of IFNγ-secreting effector $CD8^+$ T cells compared to peptide alone (Fig. 4A left), highlighting the enhanced $CD8^+$ T-cell response due to nanobody targeting via CD11b. In a similar experiment, mice were injected IP with VHH_{CD11b}-$E7_{49–57}$ or $E7_{49–57}$ conjugated to a control VHH (anti-GFP: VHH_{cont}) with adjuvant, or with adjuvant only. The control VHH-peptide adduct did not elicit a robust anti-$E7_{49–57}$ response, indicating that conjugation of the peptide to a nontargeting VHH does not enhance the antigen-specific response (Fig. 4A right).

Prophylactic vaccination with VHH_{CD11b}-$E7_{49–57}$ confers tumor-growth protection

We next evaluated whether vaccination with VHH_{CD11b}, $E7_{49–57}$ conferred protection against a subsequent tumor challenge *in vivo,* using the cell line C3.43 as the HPV cancer model. C3.43 cells are derived from the C3 line by transformation with a complete HPV16 genome-containing pRSVneo-derived plasmid (18, 19). C3.43 cells retain HPV16 E6 and E7 expression, and peptides from them are presented on MHC class I. By day 40, only one of five mice primed (day −21) and boosted (day −7) with VHH_{CD11b}-$E7_{49–57}$ and adjuvant prior to C3.43 challenge (day 0) had developed a tumor. There was therefore a significantly lower tumor burden in this group compared to that of mice receiving $E7_{49–57}$ plus adjuvant (three mice developed tumors) or adjuvant only (four mice developed tumors) ($P = 0.018$ and 0.008, respectively; Fig. 4B). The single tumor in the VHH_{CD11b}-$E7_{49–57}$ group grew more slowly than tumors of the $E7_{49–57}$ plus adjuvant and adjuvant only groups, resulting in survival until day 70 (Fig. 4C). VHH_{CD11b}-$E7_{49–57}$ conferred a significant overall survival benefit compared to that of the adjuvant-only group ($P = 0.03$; $P = 0.1$ between VHH_{CD11b}-$E7_{49–57}$ and $E7_{49–57}$ groups), whereas no difference in survival was observed between the $E7_{49–57}$ plus adjuvant and adjuvant-only groups ($P = 0.8$; Fig. 4C).

Therapeutic vaccination with VHH_{CD11b}-$E7_{49–57}$ induces tumor regression *in vivo*

We next evaluated the therapeutic potential of Ag conjugation to VHH_{CD11b}. Tumor-bearing mice were treated with VHH_{CD11b}-$E7_{49–57}$ and adjuvant, or $E7_{49–57}$ and adjuvant on days 8 and 15 after a subcutaneous challenge with C3.43 cells. Tumor growth and overall survival were monitored. The VHH_{CD11b}-$E7_{49–57}$ plus adjuvant group had a significantly lower tumor burden (7/8 mice showed complete tumor regression) than that of the $E7_{49–57}$ plus adjuvant group (4/8 mice had complete regression) ($P = 0.002$; Fig. 5A), and the survival benefit of VHH_{CD11b}-$E7_{49–57}$ over $E7_{49–57}$ trended towards significance ($P = 0.08$, Fig. 5B). No mice in the untreated group exhibited tumor regression (0/4) and all died within 40 days of challenge; thus, both the VHH_{CD11b}-$E7_{49–57}$ and $E7_{49–57}$ treatment groups provided significant survival benefits over untreated controls ($P < 0.01$). After day 40, the tumor in the one tumor-bearing mouse from the VHH_{CD11b}-$E7_{49–57}$ plus adjuvant group grew more slowly than those of tumor-bearing mice in the $E7_{49–57}$ plus adjuvant group, resulting in survival until day 75 (Fig. 5B). Mice with complete tumor regression from both the $E7_{49–57}$ and VHH_{CD11b}-$E7_{49–57}$ groups were rechallenged on the opposite flank with C3.43 tumor cells 80 days after the initial tumor challenge. None of these rechallenged mice developed

tumors, suggesting that the level of immunological memory was no different between the two groups (Fig. 5C).

We have developed methods to noninvasively image immune cell subsets *in vivo* using nanobody-based immuno-positron emission tomography (immunoPET; Fig. 5D) (24, 25). We used immunoPET to monitor $CD8^+$ tumor-infiltrating lymphocytes (TILs) in all tumor-bearing mice 15 days after tumor challenge, which was 7 days after the first vaccination for the VHH_{CD11b}-$E7_{49–57}$ and $E7_{49–57}$ groups (representative PET images are shown in Fig. 5H–5J). We saw greater TIL intensity (see Methods) in the tumors of VHH_{CD11b}-$E7_{49–57}$-treated mice compared to those in untreated mice (Fig. 5E). No obvious difference was seen when comparing the $E7_{49–57}$ and untreated groups. When stratified by TIL intensity as measured by PET (responder >5; nonresponder <5), there was a significantly lower tumor burden in responders than in nonresponders (Fig. 5G), and TIL intensity was significantly correlated with survival ($P = 0.01$), indicating the prognostic value of TILs visualized noninvasively by immunoPET. Similarly, we measured the $CD8^+$ T-cell signal intensities in the draining and contralateral lymph nodes (DLN and CLN, respectively) via immunoPET. The $CD8^+$ T-cell signal intensities in both the DLN and CLN were increased in the VHH_{CD11b}-$E7_{49–57}$ group compared to the other groups, with a significant difference observed between the DLN signal intensities of the VHH_{CD11b}-$E7_{49–57}$ and $E7_{49–57}$ groups (Fig. 5F). We hypothesized that the better induction of antigen-specific $CD8^+$ T cells in the VHH_{CD11b}-$E7_{49–57}$ group as seen by ELISpot (Fig. 4A) would yield a higher $CD8^+$ T-cell signal in the DLN of $E7^+$ tumors, where antigen-specific T cells are expected to accumulate during an antitumor response. Indeed, we found that the ratio of $CD8^+$ T-cell signal intensity in the DLN over that in the CLN was highest in the VHH_{CD11b}-$E7_{49–57}$ group (Fig. 5F gray bars). We suggest this is due to the presence of a greater number of antigen-specific T cells.

$CD11b^+$ cells are found in C3.43 tumors *in vivo*

$CD11b^+$ cells have been observed in the skin of transgenic K14E7 mice that constitutively express E7 in squamous epithelium (33). Therefore, we utilized VHH_{CD11b} as an immunoPET imaging agent in C3.43 tumor-bearing mice to test for the presence of intratumoral $CD11b^+$ cells. We labeled VHH_{CD11b} with ^{64}Cu and injected it into wild-type mice or mice harboring ~200 mm^3 (16 days after challenge) C3.43 tumors with or without VHH_{CD11b}-$E7_{49–57}$ treatment (mice were treated on day 8). C3.43 tumors were found to be positive for VHH_{CD11b}-^{64}Cu staining (Fig 6B–C). Although we do not know where exactly induction of the anti-E7 response occurs in VHH_{CD11b}-$E7_{49–57}$ vaccinated mice, a pool of Ag delivered to the tumor site may allow resident APCs to acquire it. If these APCs were to migrate to the draining lymph node, further E7-specific T cells may be recruited from that lymph node and participate in the antitumor response. Such localized delivery may be especially important when antigen levels are limiting. This imaging experiment further highlights the utility of sortase A to conjugate payloads to VHHs, as we used the identical sortase-ready VHH as a delivery vehicle for the E7 antigen in one setting, and as an immunoPET imaging agent in another.

Discussion

As HPV DNA testing becomes more widely implemented as a primary screening method for HPV infection (34), more women will test positive for high-risk HPV infection, including those with normal cytology. More than 15% of women infected with high-risk HPV strains do not initiate effective immune responses against the virus, leaving them at risk for the development of low-grade cervical intraepithelial neoplastic (CIN1) lesions (35). Although CIN1 is often eliminated by the host's immune system, regression of high-grade lesions (CIN2/3) is far less common. Progression is thus correlated with limited immune responses, increasing the risk for developing invasive cancers (36, 37). A therapeutic HPV vaccine that can stimulate the immune system to clear established HPV infections is needed, especially for patients with consecutive HPV^+ DNA tests or with CIN1 lesions, for which the only treatment option is watchful waiting (38).

We explored whether an HPV vaccine based on anti-CD11b VHH-targeted delivery of an HPV antigen-derived peptide would elicit stronger antitumor $CD8^+$ T cell responses than vaccination with peptide alone. Our data support that hypothesis. Specifically, MHC class I presentation of an ovalbumin-derived peptide was highest when conjugated to VHH_{CD11b}, compared to equimolar amounts of peptide delivered via a control VHH or as peptide alone. Other conjugates comprising VHH_{CD11b} and a different peptide should be handled similarly. The VHH_{CD11b}-$E7_{49–57}$ construct elicited a strong $CD8^+$ T-cell response *in vivo*, which afforded prophylaxis against C3.43 tumor growth. VHH_{CD11b}-$E7_{49–57}$ therapeutic vaccination induced TILs as seen in live mice by immunoPET and resulted in tumor regression and increased survival. Considerably less Ag was needed than previously reported to achieve strong $E7_{49–57}$-specific responses (i.e. 6 nmol vs. 30 nmol) when conjugated to VHH_{CD11b} (32). The approach reported here can be extended to the inclusion of multiple epitopes. Collectively, these data demonstrate that targeted delivery of HPV Ags to $CD11b^+$ cells via VHH conjugates is a viable strategy to elicit effective cellular immune responses against HPV-induced cancers. An extension to other tumor models would require the availability of a similarly immunodominant peptide, but currently such sequences are not known for other commonly studied preclinical cancer models, such as murine B16-F10 melanoma or MC-38 colon adenocarcinoma.

Other studies have shown that targeted delivery of an Ag to $CD11b^+$ cells can induce strong $CD8^+$ T-cell responses. Specifically, a detoxified form of *Bordetella pertussis* adenylate cyclase toxin (CyaA), a ligand of CD11b, has been used to deliver Ags as CyaA fusion products to elicit MHC class I– and MHC class II–restricted T-cell responses, both *in vitro* and *in vivo* (39, 40). Such CyaA-E7 fusions elicit HPV-specific $CD8^+$ T-cell responses and corresponding antitumor responses *in vivo* (41). However, the molecular mass of these CyaA fusions is ~180 kDa, which may limit access to tissues harboring appropriate $CD11b^+$ populations of APCs. In contrast, the VHH-Ag constructs are ~15 kDa, providing superior tissue penetration, even compared to conventional antibodies (~150 kDa) (42, 43). Our previous work already showed that a conventional full-size Ag-modified antibody was less efficient in eliciting Ag-specific $CD4^+$ T-cell responses than a VHH conjugated covalently to that same Ag (14). As to the use of CyaA as an alternative delivery vehicle, its bacterial origin entails the added risk of immunogenicity and the generation of CyaA-neutralizing

antibodies, which may compromise efficacy when a CyaA-based vaccine requires repeated administration. VHHs are comparatively poorly immunogenic as well (Supplementary Fig. 1), and can be humanized if necessary (44). VHH_{CD11b} binds more tightly to $CD11b^+$ cells (K_D value 0.204 ± 0.090 nM on DC2.4 cells) than CyaA (K_D 9.2 ± 4.5 and 3.2 ± 1.9 nM depending on cell type). Our previous (14) and current work shows that VHH_{CD11b}-Ag constructs have their payloads presented on MHCI. Their ease of expression, excellent tissue penetration, high affinity, and interchangeability of VHHs and Ags in VHH-Ag constructs thus create a flexible vaccine platform.

E7 expression in the skin of mice results in expansion of $CD11b^+$ cells (33). In particular, more $CD11b^+Gr1^+$ cells were present in the skin of transgenic K14E7 mice (33), which constitutively express HPV16 E7 in squamous epithelium (45). $CD11b^+Gr1^+$ cells are defined as myeloid-derived suppressor cells (MDSCs) that can show intratumoral immunosuppressive activity (46). If sites of HPV infection and/or HPV-induced cancers are at the same time foci of CD11b expression, then delivering immunodominant HPV Ags to these locations under stimulatory conditions may activate local APCs, which may also pick up other HPV Ags in addition to those delivered, thus allowing for epitope spreading. This might occur despite the immunosuppression associated with increased $CD11b^+Gr1^+$ cells, but if and how a balance between the action of stimulatory APCs and suppressive MDSCs is established in our vaccination protocol will require further study. We readily visualized the presence of $CD11b^+$ cells in E7-expressing C3.43 tumors *in vivo* via immunoPET, but it is not yet known whether these cells are associated with the observed anti-E7 immune responses in VHH_{CD11b}-$E7_{49–57}$ vaccinated mice.

Spatial resolution and imaging depth by PET is superior to bioluminescence-based *in vivo* noninvasive imaging methods such as the current *in vivo* imaging systems (IVIS), a technique not easily translatable to a clinical setting (47). Moreover, PET provides quantitative information on the distribution of label (i.e. ^{89}Zr) throughout the entire animal, with a spatial resolution of ~1 mm. Although two-photon microscopy provides better cellular and temporal resolution, it is an invasive method that requires surgical intervention, for example to expose lymph nodes for imaging, or to implant a window that allows inspection of the underlying tissue (48, 49). Multi-photon microscopy does not provide information on the distribution of label over the entire animal. We combined the spatial resolution of PET with the specificity of an anti-CD8 VHH to noninvasively visualize TILs *in vivo*. We found that TILs as seen via immunoPET were prognostic for tumor regression, in agreement with our previous work (24). These techniques could be applied to any number of cancer immunotherapy animal models and could potentially be translated to human cancers to not only provide prognostic information about treatment outcomes, but inform physicians whether patients are responding to immunotherapeutic interventions during a given course of treatment.

Supplementary Material

Refer to Web version on PubMed Central for supplementary material.

Acknowledgments

JGS was supported by the Keck School of Medicine/USC Graduate School PhD Fellowship. ELISpot plate reading was performed at the USC Immune Monitoring Core Facility supported in part by the National Cancer Institute Cancer Center Support Grant award P30CA014089. The authors also thank Jessica Ingram for providing VHH_{CD11b}.

Financial Support: AWW is supported by the Arnold O. Beckman Postdoctoral Fellowship. RWC is supported in part by funding from the Cancer Research Institute Irvington Postdoctoral Fellowship. WMK holds the Walter A. Richter Cancer Research Chair and is supported by NIH R01 CA074397. HLP is supported by the Lustgarten Foundation (award ID 388167).

References

1. Wang JW, Roden RB. Virus-like particles for the prevention of human papillomavirus-associated malignancies. Expert Rev Vaccines. 2013; 12(2):129–41. PubMed PMID: 23414405; PMCID: PMC3835148. DOI: 10.1586/erv.12.151 [PubMed: 23414405]
2. Stokley S, Jeyarajah J, Yankey D, Cano M, Gee J, Roark J, Curtis RC, Markowitz L. Human papillomavirus vaccination coverage among adolescents, 2007–2013, and postlicensure vaccine safety monitoring, 2006–2014--United States. MMWR Morbidity and mortality weekly report. 2014; 63(29):620–4. Epub 2014/07/24. PubMed PMID: 25055185. [PubMed: 25055185]
3. Brawner BM, Baker JL, Voytek CD, Leader A, Cashman RR, Silverman R, Peter N, Buchner BJ, Barnes CA, Jemmott LS, Frank I. The Development of a Culturally Relevant, Theoretically Driven HPV Prevention Intervention for Urban Adolescent Females and Their Parents/Guardians. Health Promot Pract. 2012; Epub 2012/10/27. PubMed PMID: 23099659. doi: 10.1177/1524839912462389
4. Haedicke J, Iftner T. Human papillomaviruses and cancer. Radiother Oncol. 2013; Epub 2013/07/09. PubMed PMID: 23830197. doi: 10.1016/j.radonc.2013.06.004
5. Walboomers JM, Jacobs MV, Manos MM, Bosch FX, Kummer JA, Shah KV, Snijders PJ, Peto J, Meijer CJ, Munoz N. Human papillomavirus is a necessary cause of invasive cervical cancer worldwide. JPathol. 1999; 189(1):12–9. PubMed PMID: 1. [PubMed: 10451482]
6. Stanley MA, Pett MR, Coleman N. HPV: from infection to cancer. Biochem Soc Trans. 2007; 35(Pt 6):1456–60. Epub 2007/11/23. PubMed PMID: 18031245. DOI: 10.1042/BST0351456 [PubMed: 18031245]
7. Skeate JG, Woodham AW, Einstein MH, Da Silva DM, Kast WM. Current therapeutic vaccination and immunotherapy strategies for HPV-related diseases. Hum Vaccin Immunother. 2016; 12(6): 1418–29. PubMed PMID: 26835746; PMCID: PMC4964648. DOI: 10.1080/21645515.2015.1136039 [PubMed: 26835746]
8. Bonifaz LC, Bonnyay DP, Charalambous A, Darguste DI, Fujii S, Soares H, Brimnes MK, Moltedo B, Moran TM, Steinman RM. In vivo targeting of antigens to maturing dendritic cells via the DEC-205 receptor improves T cell vaccination. J Exp Med. 2004; 199(6):815–24. PubMed PMID: 15024047; PMCID: PMC2212731. DOI: 10.1084/jem.20032220 [PubMed: 15024047]
9. Fayolle C, Osickova A, Osicka R, Henry T, Rojas MJ, Saron MF, Sebo P, Leclerc C. Delivery of multiple epitopes by recombinant detoxified adenylate cyclase of Bordetella pertussis induces protective antiviral immunity. J Virol. 2001; 75(16):7330–8. PubMed PMID: 11462005; PMCID: PMC114968. DOI: 10.1128/JVI.75.16.7330-7338.2001 [PubMed: 11462005]
10. Hamers-Casterman C, Atarhouch T, Muyldermans S, Robinson G, Hamers C, Songa EB, Bendahman N, Hamers R. Naturally occurring antibodies devoid of light chains. Nature. 1993; 363(6428):446–8. PubMed PMID: 8502296. DOI: 10.1038/363446a0 [PubMed: 8502296]
11. Arbabi Ghahroudi M, Desmyter A, Wyns L, Hamers R, Muyldermans S. Selection and identification of single domain antibody fragments from camel heavy-chain antibodies. FEBS Lett. 1997; 414(3):521–6. PubMed PMID: 9323027. [PubMed: 9323027]
12. Muyldermans S. Nanobodies: natural single-domain antibodies. Annu Rev Biochem. 2013; 82:775–97. PubMed PMID: 23495938. DOI: 10.1146/annurev-biochem-063011-092449 [PubMed: 23495938]

13. Helma J, Cardoso MC, Muyldermans S, Leonhardt H. Nanobodies and recombinant binders in cell biology. J Cell Biol. 2015; 209(5):633–44. PubMed PMID: 26056137; PMCID: PMC4460151. DOI: 10.1083/jcb.201409074 [PubMed: 26056137]

14. Duarte JN, Cragnolini JJ, Swee LK, Bilate AM, Bader J, Ingram JR, Rashidfarrokhi A, Fang T, Schiepers A, Hanke L, Ploegh HL. Generation of Immunity against Pathogens via Single-Domain Antibody-Antigen Constructs. J Immunol. 2016; 197(12):4838–47. PubMed PMID: 27821668. DOI: 10.4049/jimmunol.1600692 [PubMed: 27821668]

15. Arnaout MA. Structure and function of the leukocyte adhesion molecules CD11/CD18. Blood. 1990; 75(5):1037–50. PubMed PMID: 1968349. [PubMed: 1968349]

16. Popp MW, Ploegh HL. Making and breaking peptide bonds: protein engineering using sortase. Angew Chem Int Ed Engl. 2011; 50(22):5024–32. PubMed PMID: 21538739. DOI: 10.1002/anie.201008267 [PubMed: 21538739]

17. Popp MW, Antos JM, Grotenbreg GM, Spooner E, Ploegh HL. Sortagging: a versatile method for protein labeling. Nat Chem Biol. 2007; 3(11):707–8. PubMed PMID: 17891153. DOI: 10.1038/nchembio.2007.31 [PubMed: 17891153]

18. Feltkamp MC, Smits HL, Vierboom MP, Minnaar RP, de Jongh BM, Drijfhout JW, ter Schegget J, Melief CJ, Kast WM. Vaccination with cytotoxic T lymphocyte epitope-containing peptide protects against a tumor induced by human papillomavirus type 16-transformed cells. Eur J Immunol. 1993; 23(9):2242–9. PubMed PMID: 7690326. DOI: 10.1002/eji.1830230929 [PubMed: 7690326]

19. Smith KA, Meisenburg BL, Tam VL, Pagarigan RR, Wong R, Joea DK, Lantzy L, Carrillo MA, Gross TM, Malyankar UM, Chiang CS, Da Silva DM, Kundig TM, Kast WM, Qiu Z, Bot A. Lymph node-targeted immunotherapy mediates potent immunity resulting in regression of isolated or metastatic human papillomavirus-transformed tumors. Clin Cancer Res. 2009; 15(19):6167–76. PubMed PMID: 19789304; PMCID: PMC2756704. DOI: 10.1158/1078-0432.CCR-09-0645 [PubMed: 19789304]

20. Guimaraes CP, Witte MD, Theile CS, Bozkurt G, Kundrat L, Blom AE, Ploegh HL. Site-specific C-terminal and internal loop labeling of proteins using sortase-mediated reactions. Nat Protoc. 2013; 8(9):1787–99. PubMed PMID: 23989673; PMCID: PMC3943461. DOI: 10.1038/nprot.2013.101 [PubMed: 23989673]

21. Theile CS, Witte MD, Blom AE, Kundrat L, Ploegh HL, Guimaraes CP. Site-specific N-terminal labeling of proteins using sortase-mediated reactions. Nat Protoc. 2013; 8(9):1800–7. Epub 2013/08/31. PubMed PMID: 23989674; PMCID: 3941705. DOI: 10.1038/nprot.2013.102 [PubMed: 23989674]

22. Kirchhofer A, Helma J, Schmidthals K, Frauer C, Cui S, Karcher A, Pellis M, Muyldermans S, Casas-Delucchi CS, Cardoso MC, Leonhardt H, Hopfner KP, Rothbauer U. Modulation of protein properties in living cells using nanobodies. Nat Struct Mol Biol. 2010; 17(1):133–8. PubMed PMID: 20010839. DOI: 10.1038/nsmb.1727 [PubMed: 20010839]

23. Yan L, Woodham AW, Da Silva DM, Kast WM. Functional analysis of HPV-like particle-activated Langerhans cells in vitro. Methods Mol Biol. 2015; 1249:333–50. Epub 2014/10/29. PubMed PMID: 25348318. DOI: 10.1007/978-1-4939-2013-6_25 [PubMed: 25348318]

24. Rashidian M, Ingram JR, Dougan M, Dongre A, Whang KA, LeGall C, Cragnolini JJ, Bierie B, Gostissa M, Gorman J, Grotenbreg GM, Bhan A, Weinberg RA, Ploegh HL. Predicting the response to CTLA-4 blockade by longitudinal noninvasive monitoring of CD8 T cells. J Exp Med. 2017; 214(8):2243–55. PubMed PMID: 28666979; PMCID: PMC5551571. DOI: 10.1084/jem.20161950 [PubMed: 28666979]

25. Rashidian M, Keliher EJ, Bilate AM, Duarte JN, Wojtkiewicz GR, Jacobsen JT, Cragnolini J, Swee LK, Victora GD, Weissleder R, Ploegh HL. Noninvasive imaging of immune responses. Proc Natl Acad Sci U S A. 2015; 112(19):6146–51. Epub 2015/04/23. PubMed PMID: 25902531; PMCID: 4434737. DOI: 10.1073/pnas.1502609112 [PubMed: 25902531]

26. Feltkamp MC, Vreugdenhil GR, Vierboom MP, Ras E, van der Burg SH, ter Schegget J, Melief CJ, Kast WM. Cytotoxic T lymphocytes raised against a subdominant epitope offered as a synthetic peptide eradicate human papillomavirus type 16-induced tumors. Eur J Immunol. 1995; 25(9):2638–42. PubMed PMID: 7589138. DOI: 10.1002/eji.1830250935 [PubMed: 7589138]

27. Kanodia S, Da Silva DM, Karamanukyan T, Bogaert L, Fu YX, Kast WM. Expression of LIGHT/TNFSF14 combined with vaccination against human papillomavirus Type 16 E7 induces significant tumor regression. Cancer Research. 2010; 70(10):3955–64. Epub 2010/05/13. PubMed PMID: 20460520; PMCID: 2873073. DOI: 10.1158/0008-5472.CAN-09-3773 [PubMed: 20460520]
28. Velders MP, Weijzen S, Eiben GL, Elmishad AG, Kloetzel PM, Higgins T, Ciccarelli RB, Evans M, Man S, Smith L, Kast WM. Defined flanking spacers and enhanced proteolysis is essential for eradication of established tumors by an epitope string DNA vaccine. J Immunol. 2001; 166(9): 5366–73. PubMed PMID: 11313372. [PubMed: 11313372]
29. Blum JS, Wearsch PA, Cresswell P. Pathways of antigen processing. Annu Rev Immunol. 2013; 31:443–73. PubMed PMID: 23298205; PMCID: PMC4026165. DOI: 10.1146/annurev-immunol-032712-095910 [PubMed: 23298205]
30. Clarke SR, Barnden M, Kurts C, Carbone FR, Miller JF, Heath WR. Characterization of the ovalbumin-specific TCR transgenic line OT-I: MHC elements for positive and negative selection. Immunol Cell Biol. 2000; 78(2):110–7. PubMed PMID: 10762410. DOI: 10.1046/j.1440-1711.2000.00889.x [PubMed: 10762410]
31. Joffre OP, Segura E, Savina A, Amigorena S. Cross-presentation by dendritic cells. Nat Rev Immunol. 2012; 12(8):557–69. PubMed PMID: 22790179. DOI: 10.1038/nri3254 [PubMed: 22790179]
32. Barrios K, Celis E. TriVax-HPV: an improved peptide-based therapeutic vaccination strategy against human papillomavirus-induced cancers. Cancer Immunol Immunother. 2012; 61(8):1307–17. PubMed PMID: 22527249; PMCID: PMC3446251. DOI: 10.1007/s00262-012-1259-8 [PubMed: 22527249]
33. Damian-Morales G, Serafin-Higuera N, Moreno-Eutimio MA, Cortes-Malagon EM, Bonilla-Delgado J, Rodriguez-Uribe G, Ocadiz-Delgado R, Lambert PF, Gariglio P. The HPV16 E7 Oncoprotein Disrupts Dendritic Cell Function and Induces the Systemic Expansion of CD11b(+)Gr1(+) Cells in a Transgenic Mouse Model. Biomed Res Int. 2016; 2016:8091353. PubMed PMID: 27478837; PMCID: PMC4958469. doi: 10.1155/2016/8091353 [PubMed: 27478837]
34. Abraham J, Stenger M. Cobas HPV test for first-line screening for cervical cancer. J Community Support Oncol. 2014; 12(5):156–7. Epub 2014/06/28. PubMed PMID: 24971425. [PubMed: 24971425]
35. Giuliano AR, Harris R, Sedjo RL, Baldwin S, Roe D, Papenfuss MR, Abrahamsen M, Inserra P, Olvera S, Hatch K. Incidence, prevalence, and clearance of type-specific human papillomavirus infections: The Young Women's Health Study. J Infect Dis. 2002; 186(4):462–9. Epub 2002/08/27. PubMed PMID: 12195372. DOI: 10.1086/341782 [PubMed: 12195372]
36. Rodriguez AC, Schiffman M, Herrero R, Wacholder S, Hildesheim A, Castle PE, Solomon D, Burk R. Proyecto Epidemiologico Guanacaste G. Rapid clearance of human papillomavirus and implications for clinical focus on persistent infections. J Natl Cancer Inst. 2008; 100(7):513–7. PubMed PMID: 18364507; PMCID: PMC3705579. DOI: 10.1093/jnci/djn044 [PubMed: 18364507]
37. Walker JL, Wang SS, Schiffman M, Solomon D. Predicting absolute risk of CIN3 during post-colposcopic follow-up: results from the ASCUS-LSIL Triage Study (ALTS). Am J Obstet Gynecol. 2006; 195(2):341–8. Epub 2006/08/08. PubMed PMID: 16890545. DOI: 10.1016/j.ajog.2006.02.047 [PubMed: 16890545]
38. Massad LS, Einstein MH, Huh WK, Katki HA, Kinney WK, Schiffman M, Solomon D, Wentzensen N, Lawson HW. 2012 updated consensus guidelines for the management of abnormal cervical cancer screening tests and cancer precursors. Obstet Gynecol. 2013; 121(4):829–46. Epub 2013/05/03. PubMed PMID: 23635684. DOI: 10.1097/AOG.0b013e3182883a34 [PubMed: 23635684]
39. Guermonprez P, Khelef N, Blouin E, Rieu P, Ricciardi-Castagnoli P, Guiso N, Ladant D, Leclerc C. The adenylate cyclase toxin of Bordetella pertussis binds to target cells via the alpha(M)beta(2) integrin (CD11b/CD18). J Exp Med. 2001; 193(9):1035–44. PubMed PMID: 11342588; PMCID: PMC2193436. [PubMed: 11342588]

40. Loucka J, Schlecht G, Vodolanova J, Leclerc C, Sebo P. Delivery of a MalE CD4(+)-T-cell epitope into the major histocompatibility complex class II antigen presentation pathway by Bordetella pertussis adenylate cyclase. Infect Immun. 2002; 70(2):1002–5. PubMed PMID: 11796640; PMCID: PMC127677. [PubMed: 11796640]
41. Esquerre M, Bouillette-Marussig M, Goubier A, Momot M, Gonindard C, Keller H, Navarro A, Bissery MC. GTL001, a bivalent therapeutic vaccine against human papillomavirus 16 and 18, induces antigen-specific CD8+ T cell responses leading to tumor regression. PLoS One. 2017; 12(3):e0174038. PubMed PMID: 28301611; PMCID: PMC5354464. doi: 10.1371/journal.pone.0174038 [PubMed: 28301611]
42. Smolarek D, Bertrand O, Czerwinski M. Variable fragments of heavy chain antibodies (VHHs): a new magic bullet molecule of medicine? Postepy Hig Med Dosw (Online). 2012; 66:348–58. Epub 2012/06/19. PubMed PMID: 22706121. [PubMed: 22706121]
43. Hassanzadeh-Ghassabeh G, Devoogdt N, De Pauw P, Vincke C, Muyldermans S. Nanobodies and their potential applications. Nanomedicine (Lond). 2013; 8(6):1013–26. PubMed PMID: 23730699. DOI: 10.2217/nnm.13.86 [PubMed: 23730699]
44. Vincke C, Loris R, Saerens D, Martinez-Rodriguez S, Muyldermans S, Conrath K. General strategy to humanize a camelid single-domain antibody and identification of a universal humanized nanobody scaffold. J Biol Chem. 2009; 284(5):3273–84. PubMed PMID: 19010777. DOI: 10.1074/jbc.M806889200 [PubMed: 19010777]
45. Herber R, Liem A, Pitot H, Lambert PF. Squamous epithelial hyperplasia and carcinoma in mice transgenic for the human papillomavirus type 16 E7 oncogene. J Virol. 1996; 70(3):1873–81. PubMed PMID: 8627712; PMCID: PMC190015. [PubMed: 8627712]
46. Gabrilovich DI, Nagaraj S. Myeloid-derived suppressor cells as regulators of the immune system. Nat Rev Immunol. 2009; 9(3):162–74. PubMed PMID: 19197294; PMCID: PMC2828349. DOI: 10.1038/nri2506 [PubMed: 19197294]
47. Zinn KR, Chaudhuri TR, Szafran AA, O'Quinn D, Weaver C, Dugger K, Lamar D, Kesterson RA, Wang X, Frank SJ. Noninvasive bioluminescence imaging in small animals. ILAR J. 2008; 49(1):103–15. PubMed PMID: 18172337; PMCID: PMC2614121. [PubMed: 18172337]
48. Dzhagalov IL, Melichar HJ, Ross JO, Herzmark P, Robey EA. Two-photon imaging of the immune system. Curr Protoc Cytom. 2012; Chapter 12(Unit12):26. PubMed PMID: 22470153; PMCID: PMC3662370. doi: 10.1002/0471142956.cy1226s60
49. Helmchen F, Denk W. Deep tissue two-photon microscopy. Nat Methods. 2005; 2(12):932–40. PubMed PMID: 16299478. DOI: 10.1038/nmeth818 [PubMed: 16299478]

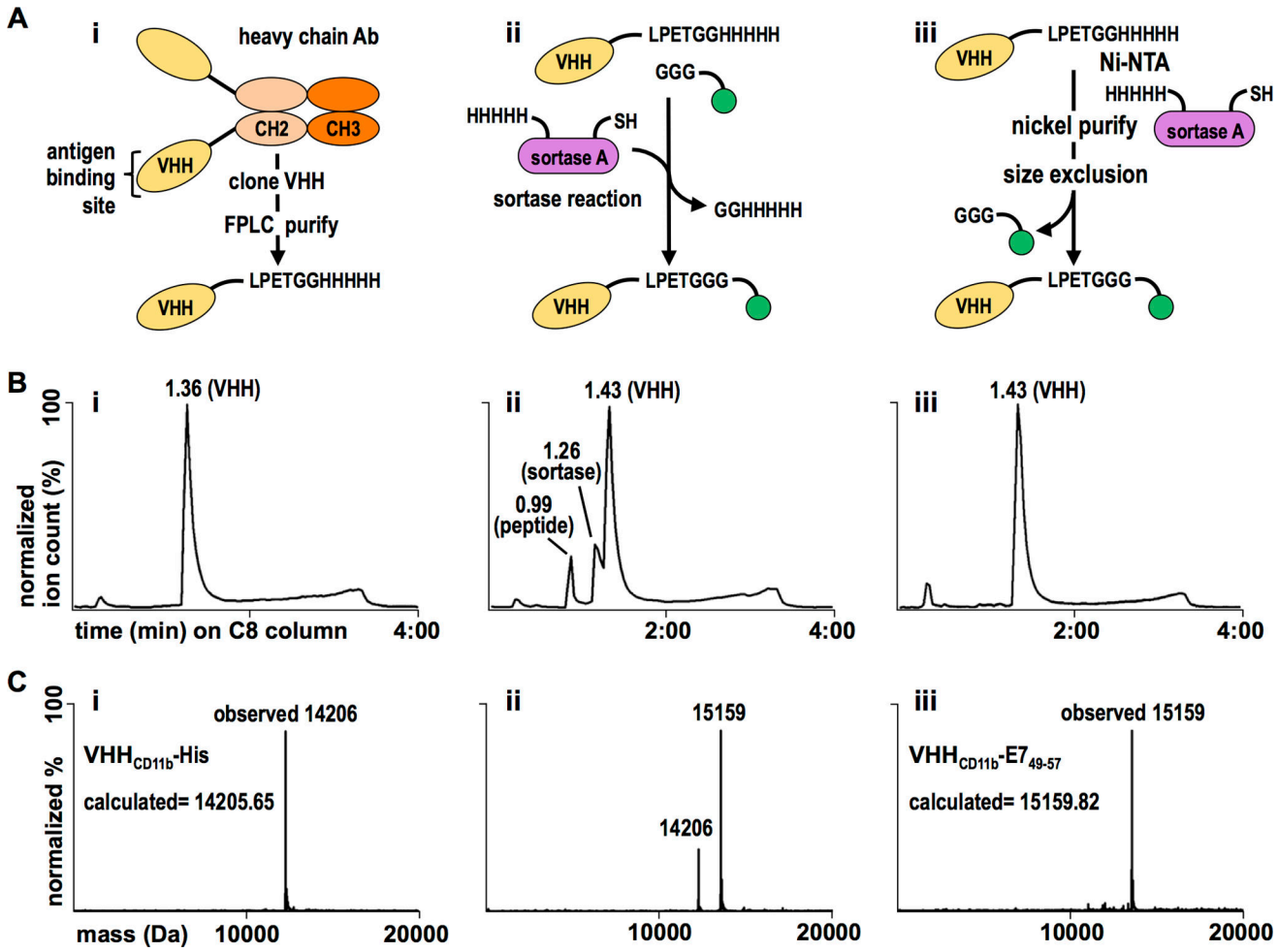

Figure 1.

VHH$_{CD11b}$-E7$_{49–57}$ conjugate design, purification, and validation. A) i. VHH$_{CD11b}$ (yellow) was cloned from the VHH genes of an immunized alpaca, expressed with a C-terminal sortase-recognition motif (LPETG), and purified via FPLC. ii. The E7$_{49–57}$ antigen (green) was synthesized with a G_3 motif, and was site-specifically conjugated to VHH$_{CD11b}$ via a sortase A (purple)-mediated reaction. iii. The reaction mixture was purified in two steps. First, Ni-NTA beads were used to remove His-tag containing sortase A and unreacted VHH$_{CD11b}$. Second, size exclusion was used to remove unreacted E7$_{49–57}$ antigen. B) Chromatograms showing the retention times of different species on a C8 HPLC column of (i) the purified sortase-ready VHH, (ii) the complete reaction mixture, and (iii) the final product following two-step purification. C i–iii) The calculated and observed mass(es) of the primary peaks (at 1.36, 1.43, and 1.43 min in the panels above, respectively) of the corresponding HPLC chromatograms.

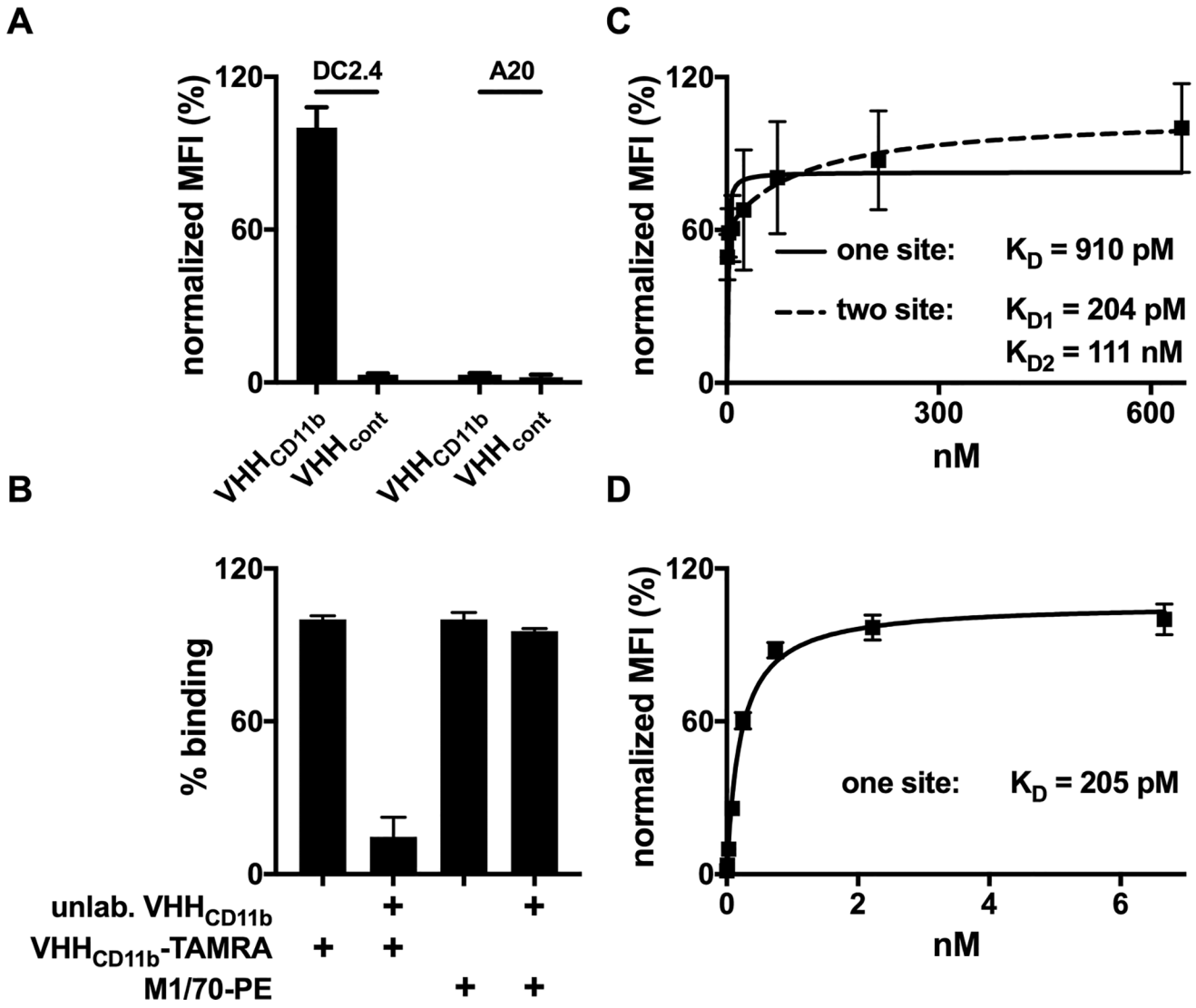

Figure 2.

Binding of VHH_{CD11b} to $CD11b^+$ cells. A) $CD11b^+$ DC2.4 cells or $CD11b^-$ A20 cells were incubated with TAMRA-labeled VHH_{CD11b} or VHH_{cont} (anti-GFP control VHH). The mean fluorescence intensity (MFI) as assessed by cytofluorimetry was normalized to the average maximum observed MFI of VHH_{CD11b}-TAMRA on DC2.4 cells. B) DC2.4 cells were pre-incubated with unlabeled VHH_{CD11b} (10 μg/mL) for 30 min at 4°C, and then stained with VHH_{CD11b}-TAMRA or M1/70-PE for 30 min at 4°C. MFI was assessed via cytofluorimetry and binding was normalized to those observed with VHH_{CD11b}-TAMRA (left 2 columns) or M1/70-PE (right 2 columns). C–D) DC2.4 cells were incubated with different concentrations of VHH_{CD11b}-TAMRA (C) or M170-PE (D) for and 30 min at 4°, and the MFI as assessed by cytofluorimetry was normalized to the maximum observed MFI for VHH_{CD11b}-TAMRA or M170-PE, respectively. One-site (solid) or two-site (dashed) hyperbolic binding models were then used to calculate relative K_D values. All data shown are representatives of at least two independent experiments performed in triplicate (mean ± SD).

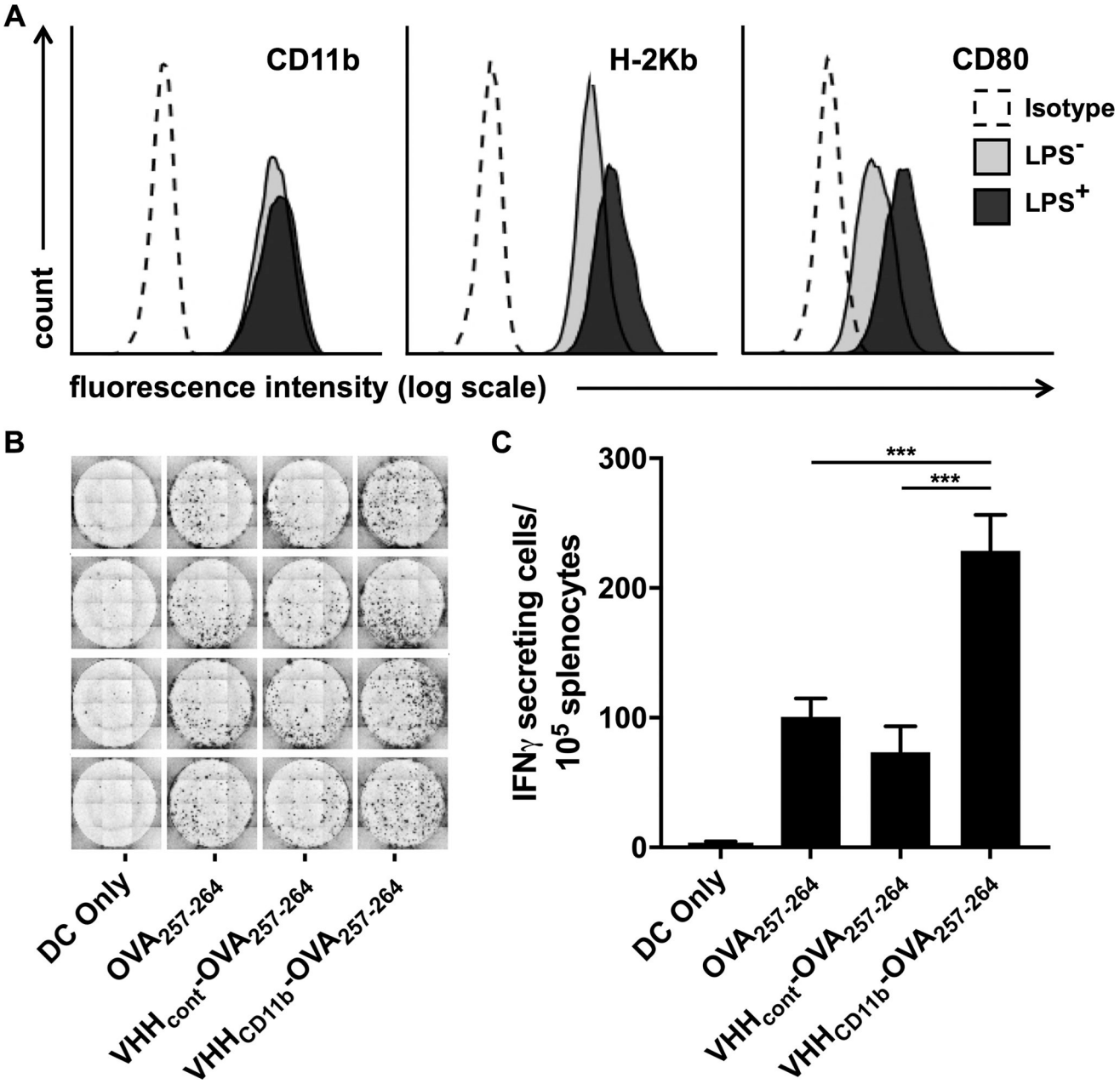

Figure 3.

Antigen presentation is increased with VHH_{CD11b}. A) DC2.4 cells express CD11b, H-2Kb (MHCI known to present $OVA_{257–264}$), and CD80 (costimulatory molecule) as assessed via cytofluorimetry (light gray histograms). Isotype controls (Isotype) are shown as empty dashed histograms. CD80 and H-2Kb expression were increased following 24-hr incubation with LPS (dark gray histograms). B-C) DC2.4 cells were treated as indicated before LPS stimulation, followed by coculture with splenocytes from a $RAG^{-/-}$ OT-I mouse (1 DC2.4 cell: 20 OT-I splenocytes), and the number of IFNγ-secreting cells was measured via ELISpot assay. The spots shown in B are quantified in C (means ± SD are shown; ***$P <$

0.001) of an experiment performed in quadruplicate, and is a representative to three independent experiments.

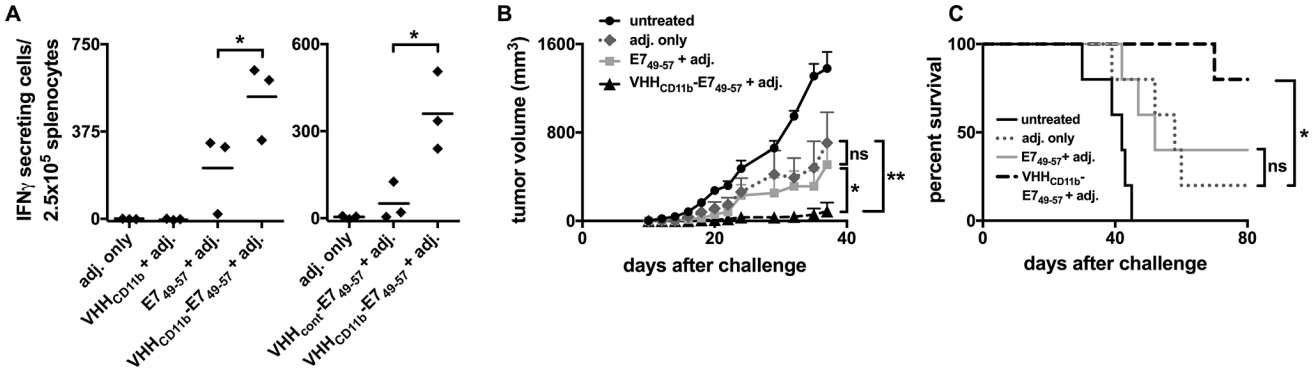

Figure 4.

VHH_{CD11b}-$E7_{49–57}$ vaccine-induced HPV-specific T-cell responses and VHH_{CD11b}-$E7_{49–57}$ vaccine-induced protection against C3.43 tumor growth *in vivo.* A) Wild-type C57BL/6 mice were injected IP with VHH_{CD11b}, $E7_{49–57}$, or VHH_{CD11b}-$E7_{49–57}$ plus adjuvant (adj. = 50 μg Poly(I:C) + 50 μg agonistic anti-CD40 Ab), or adj. only (left panel). 14-days post-vaccination, spleens were harvested and anti-$E7_{49–57}$ specific $CD8^+$ T cells were enumerated via IFNγ ELISpot. In a separate experiment, mice were injected IP with 6 nmol VHH_{CD11b}-$E7_{49–57}$ or VHH_{cont} (anti-GFP VHH)-$E7_{49–57}$ plus adj., or adj. only 14 days prior to IFNγ ELISpot assay (right panel). Horizontal bars indicate the average number of spots per group from one of two experiments ($n = 3$ per group per experiment; $^*P < 0.05$). B–C) Wild-type C57BL/6 mice were injected IP with VHH_{CD11b}, $E7_{49–57}$, or VHH_{CD11b}-$E7_{49–57}$ plus adj., or adj. only on days −21 and −7 or left untreated ($n = 5$ per group). On day 0, mice were challenged with 3×10^5 C3.43 cells. Tumor growth (C) and survival (D) were monitored, and shown is the average group means from one of two independent experiments (group means ± SEM are shown; $^*P < 0.05$, $^{**}P < 0.01$).

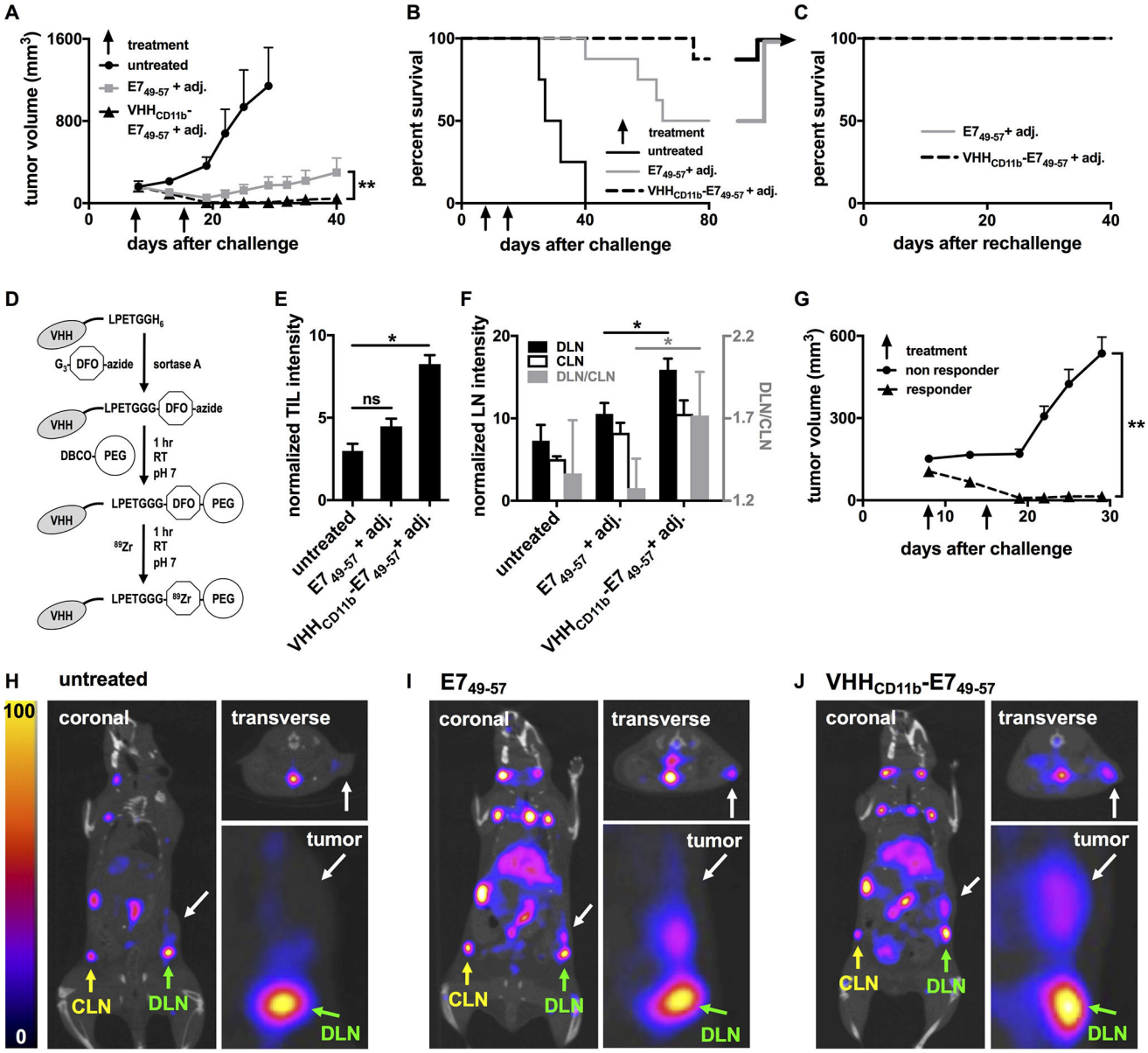

Figure 5.

VHH_{CD11b}-$E7_{49–57}$ vaccine induced responses in tumor-bearing mice *in vivo.* A–B) Wild-type C57BL/6 mice were challenged with 3×10^5 C3.43 cells on day 0 resulting in palpable tumors (~200 mm^3) on day 8. Mice were then injected IP with $E7_{49–57}$ ($n = 8$) or VHH_{CD11b}-$E7_{49–57}$ ($n = 8$) plus adj. on days 8 and 15, or left untreated ($n = 4$). Tumor growth (A) and survival were monitored (means ± SEM are shown; $^{**}P < 0.01$ as assessed by an unpaired *t* test). C) Mice with complete tumor regression from $E7_{49–57}$ or VHH_{CD11b}-$E7_{49–57}$ groups in (B) were rechallenged 80 days after the initial challenge with 3×10^5 C3.43 cells contralaterally and survival was monitored ($n = 3$ per group). D) Schematic of ^{89}Zr-labeled VHHs preparation for immunoPET imaging (DFO: desferoxamine; PEG: polyethylene glycol). E–F) All tumor-bearing mice from A were injected via the tail vein with VHH_{CD8}-^{89}Zr on day 15 and $CD8^+$ T cells were imaged *in vivo* on day 16 by PET-CT

on the same day. TIL, draining lymph node (DLN), and contralateral lymph node (CLN) $CD8^+$ T-cell intensities from the PET images were quantified (means ± SEM are shown; $*P < 0.05$). The ratios of the intensities in the DLN to CLN shown in F (gray bars) are plotted according to the right y-axis (shown in gray). G) Tumor growth was stratified by TIL intensity (responder TIL intensity >5 ($n = 9$); nonresponder <5 ($n = 11$); means ± SEM are shown; $**P < 0.001$). H–J) Representative PET-CT images from the untreated group (H), $E7_{49–57}$ + adj. group (I), and VHH_{CD11b}-$E7_{49–57}$ + adj. group (J) from one of two independent experiments. White arrows in the coronal (left), insets from the coronal (lower right), and transverse (upper right) images indicate the sites of the tumors. Green and yellow arrows indicate the sites of the DLN and CLN, respectively.

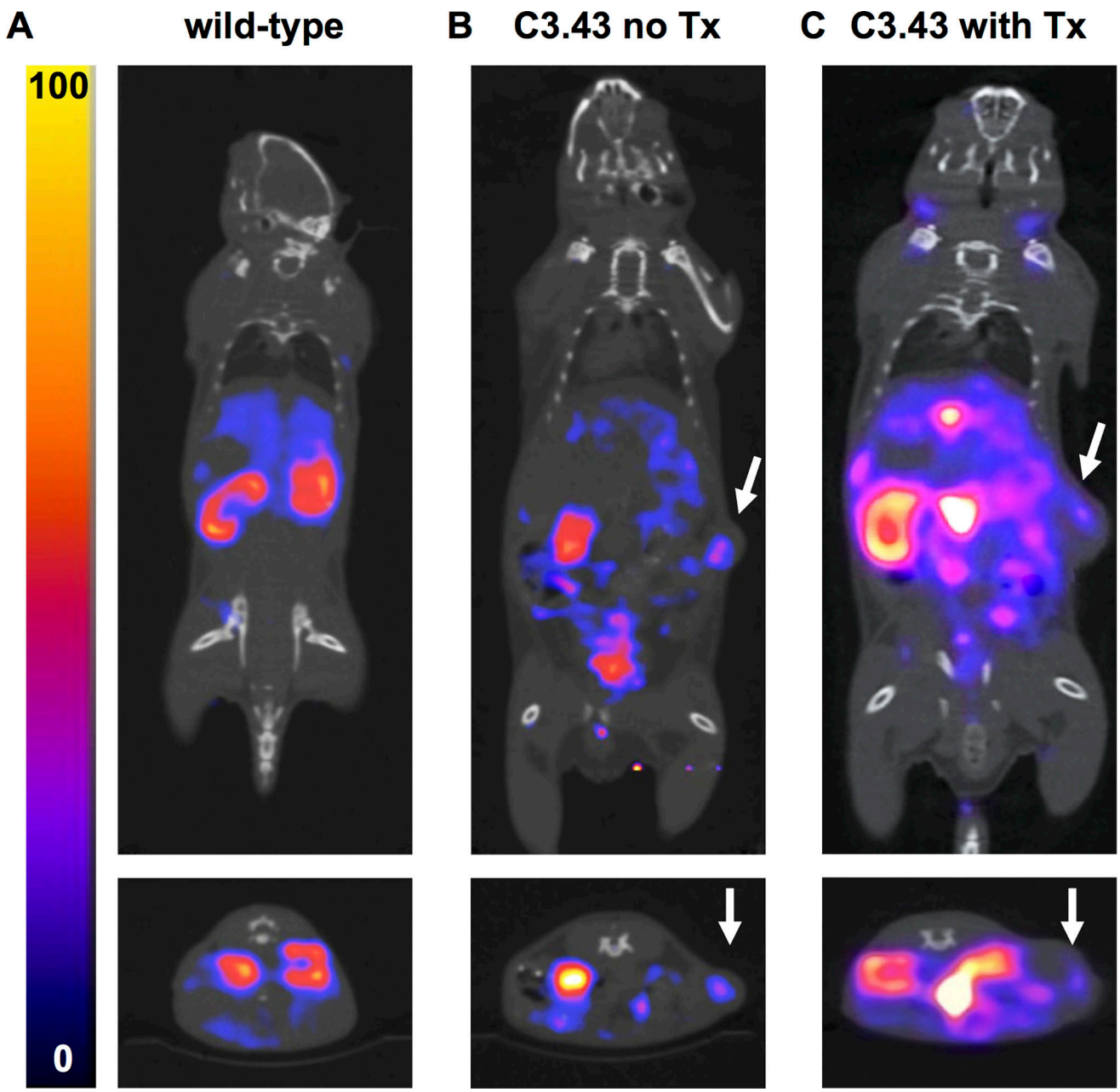

Figure 6.

ImmunoPET analysis of CD11b^{+} cells *in vivo*. Wild-type mice or mice challenged with 3×10^{5} C3.43 cells 16 days prior (with or without VHH_{CD11b}-$E7_{49–57}$ treatment (Tx) on day 8) were injected via the tail vein with VHH_{CD11b}-^{64}Cu and imaged by PET-CT ($n = 4$ per group). Representative PET-CT images from A) wild-type, B) C3.43 tumor-bearing without Tx, and C) C3.43 tumor-bearing with Tx animals are shown from two independent experiments. Images from A and B were collected on the same day, and C was acquired on a separate day. White arrows in the coronal (top), and transverse (bottom) images indicate the sites of the tumors.